An Overview of the 3D Simulation Efforts at Arizona State University Directed Towards Understanding Transport in the Quantum Dots and the Ultra-Small Devices of the Future*

Richard Akis, Dragica Vasileska and David K. Ferry

Department of Electrical Engineering
Arizona State University, Tempe AZ 85287-5706, USA
richard.akis@asu.edu, vasilesk@imap2.asu.edu, ferry@asu.edu

ABSTRACT

A brief summary of some of the simulation efforts within the Nanostructure Research Group at Arizona State University is presented, with emphasis on the tools used for modeling deep-submicrometer devices and quantum dot structures under low bias conditions. The results obtained with our 3D drift-diffusion simulator for 0.1 μm *n*-channel MOSFETs show that the atomistic nature of the impurity atoms has significant influence on the device transfer characteristics. In the case of quantum dot structures, we find that the level quantization is preserved even as the dot is opened, but that there is a selection of particular eigenstates that depends strongly on the positions of the contacts.

Keywords: scaled Si-MOSFETs, discrete impurities, threshold voltage, quantum dots, ballistic transport.

INTRODUCTION

The demand for speed, performance and cost effectiveness continues to push semiconductor devices towards the limits of miniaturization. In these ultra-small devices of the future, random microscopic fluctuations in the number and location of the dopant atoms induce inhomogeneities in the potential and the field pattern among a large number of what should be identical devices, thus causing intrinsic variation in their threshold voltage and drain current characteristics. The potential fluctuations, which lead to further electron confinement into quantum dots, naturally bring one from the problem of modeling ultra-small devices to the problem of also understanding transport in single and coupled quantum dot structures [1]. The latter have been the focus of numerous studies as well. For example, controllable loading of these dots with few electrons has been achieved, thus allowing one to speak of artificial quantum-dot hydrogen atoms, quantum-dot helium atoms, etc. Usually arrays of such dots are prepared on semiconductor heterostructures, such that all of them contain the same number of electrons. Experimental conditions not only allow the number of electrons per dot to be tuned, thus switching from one quantum dot element to another, but also determine whether the individual atoms are isolated or coupled with each other [2].

Along with these rather exciting technological trends, the difficulties associated with the fabrication of future ultra-small devices and the quantum dot structures are putting new demands to the area of computational electronics. For this purpose, during the course of several years we have developed a number of simulation tools, including 3D drift-diffusion simulators, 3D Schrödinger-Poisson solvers, 3D Monte Carlo particle-based simulators and a 2D quantum simulator based on a variation of the cascading scattering matrix technique.

The 3D drift-diffusion simulator has been successfully used in understanding the fluctuations of the subthreshold current, turn-off voltage and threshold voltage in MOSFETs with 0.1 μm gate-lengths [3]. What concerns our 3D Monte Carlo particle-based simulator, discussed in details in [4], it is unique in the way we include the electron-electron and electron-impurity interactions. Our real-space scheme automatically incorporates screening, simultaneous scattering from different impurity atoms and avoids the problem of double counting of a portion of the short-range Coulomb force (which has traditionally been incorporated in the **k**-space portion of the Monte Carlo transport kernel). The excellent agreement between our simulation mobility results with the experimental data for variable resistor doping levels, proves the correctness of our novel approach.

The self-consistent confining potentials and discrete energy levels in a variety of quantum dot structures fabricated in both GaAs and Si technology have been calculated using our 3D Schrödinger-Poisson Solvers [5,6]. For GaAs/AlGaAs quantum dots [5], simulation results for the activation barrier height and the number of electrons in the dot are in agreement with those utilized in the energy balance analysis for similar structure investigated experimentally in connection with negative conductance behavior.

With regards to the discrete energy levels of quantum dots, we found that a specific set of eigenstates, those scarred by classical periodic orbits, can play an important

* This work was supported in part by NSF under Contract No. ECS-9802596 and by ONR under Contract No. N00014-99-1-0318.

role in ballistic transport in the low bias regime. In particular, we find that these scarred states are maintained even when the dot is opened up with several propagating modes in the quantum point contacts (QPCs).

DISCRETE IMPURITY EFFECTS IN DEEP-SUBMICROMETER MOSFETS

The standard 3D drift-diffusion model was used in this study. We use finite-difference discretization and employ a decoupled scheme for the numerical solution of the resulting set of nonlinear equations. Briefly, the linearized Poisson equation is repeatedly solved for the improved value of the electrostatic potential ϕ. The resulting values for ϕ are then used to obtain the improved values for the electron and hole density n and p. The above procedure is repeated until self-consistent values for ϕ, n and p are obtained. We use Stone's Strongly Implicit Procedure [7] for the numerical solution of the 3D Poisson equation and employ the Bi-CGSTAB method [8] with ILU(0) preconditioner for the solution of the electron current continuity equation.

The geometrical and structural parameters of the device modeled are as follows: gate-length L_G =0.1 μm, gate-width W_G =0.05 μm and oxide thickness t_{ox} =3 nm. The substrate doping is N_A =8×10^{17} cm^{-3}, whereas the doping of the source and drain regions is N_D =10^{19} cm^{-3}. The length of the discrete doping region equals L_G, whereas the depth and the width of the discrete doping region is 58.6 nm and 86.9 nm, respectively. Due to the high doping densities used in these simulations, the 3D Poisson and 3D electron current continuity equation are solved assuming Fermi-Dirac (degenerate) statistics with D_n and μ_n constant (μ_n =300 cm^2/V-s). The procedure used for generating the atomistic impurity distribution in the discrete doping region of the device is described in [9].

A set of 20 transfer characteristics for devices with different number and different distribution of the impurity atoms under the gate is shown in Fig. 1a. For comparison, we also show the continuum doping model results. As discussed in [9], the spread of the transfer characteristics along the gate axis is associated to the non-uniformity of the potential barrier (see Fig. 2), which allows for early turn-on of some parts of the channel. Based on the results shown in Fig. 1a, statistical characterization was made for two very important device parameters: threshold voltage V_{th} (equal to the gate voltage V_G for which I_D =10^{-7} A) and turn-off voltage V_{off} (equal to V_G for which I_D =10^{-10} A). The standard deviation for both V_{th} and V_{off} is calculated to be 25.8 mV and 23.8 mV, respectively. It is important to note that the device transfer characteristics were not significantly affected with the introduction of discrete doping regions in the n^+ source and drain regions.

We also observed a significant correlation between the number of dopants in the part of the discrete doping region that extends down to 7.2 nm from the semiconductor-oxide interface and the magnitude of V_{th} (see Fig. 1b). The value of the correlation factor dropped to about half this value when taking into account the number of atoms that fall within the total discrete doping region. The results for the depth dependence of the correlation factor shown in Fig. 1c, confirm these observations. It is clear that it is not the total number of dopants that affects the magnitude of V_{th}, but it is the number of dopant atoms that fall within the first 30-40 nm that are relevant.

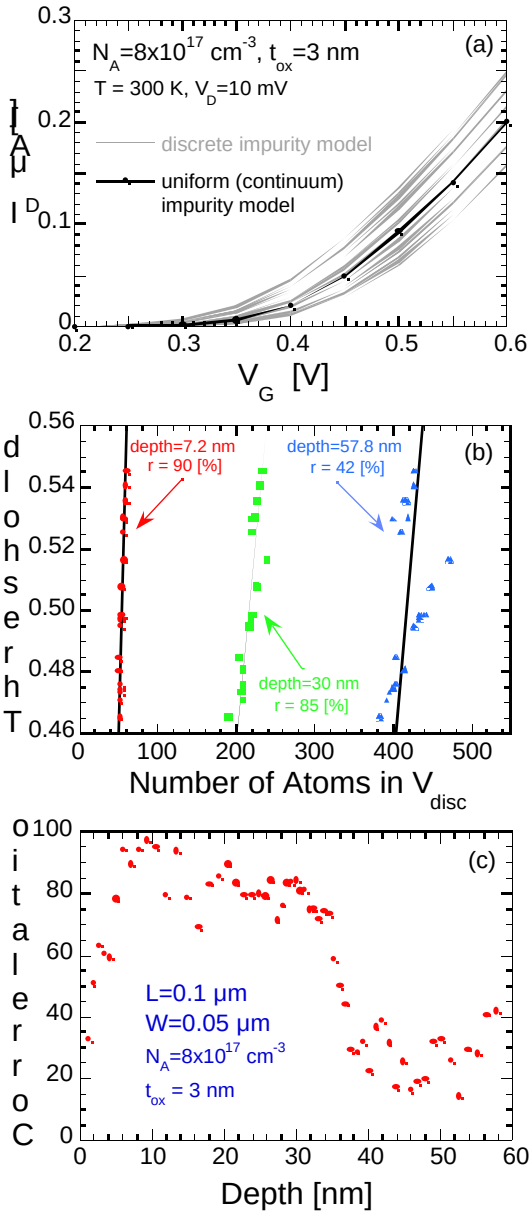

Figure 1: (a) MOSFET transfer characteristics. (b) V_{th} versus number of atoms. Parameter is the depth of the discrete doping region taken into consideration. (c) Depth-dependence of the correlation factor.

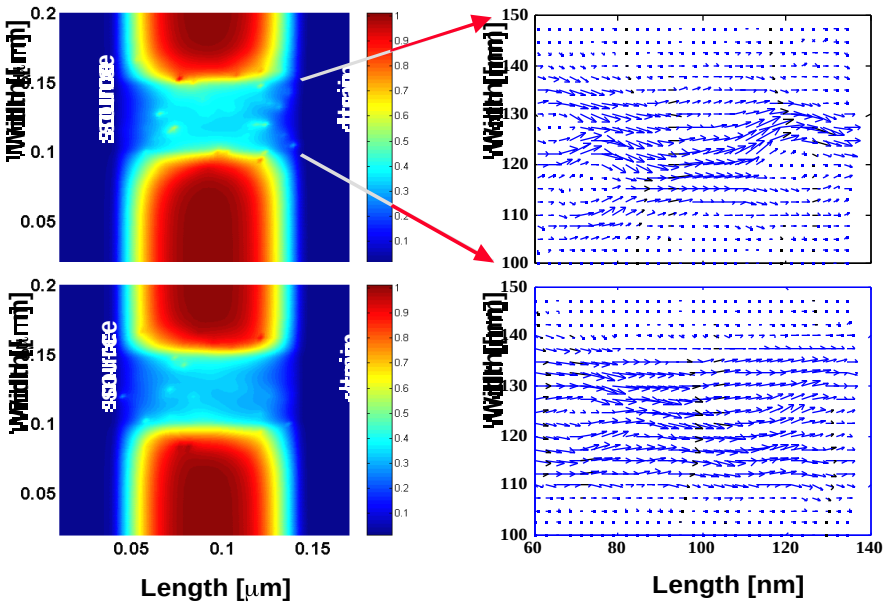

Figure 2: The effect of the randomly sited impurities can be seen on the potential plots on the left for two devices with different impurity distribution. The potential fluctuations force the current to divert around the potential peak of the random impurity. This may be seen on the figures on the right where the current flow vectors avoid several regions, which represent the role of the impurities. The device gate-length is 0.1 μm and its gate-width is 0.05 μm.

MODELING OF OPEN QUANTUM DOTS

A very important issue with regards to open quantum dots is the level broadening of energy levels. Recently, studies of magnetotransport fluctuations in open circular quantum dots have used simple tunneling models in order to explain the results [10,11]. The conclusion drawn was that the periodic nature of the fluctuations could be understood almost exclusively in terms of the density of states of a closed dot, even when several modes passed through the QPCs. On the other hand, much of the semi-classical theory of open quantum dots begins with the crucial assumption that the openness of the dot broadens the levels sufficiently that quantization is no longer important in determining dot behavior [12]. Simulating quantum dots that have a realistic soft potential obtained from a self-consistent calculation, we find that an intermediate situation arises - the level quantization is preserved in the open dots, but is done in a highly selective manner which depends strongly on the positions of the QPCs.

The dot in question is defined by a split gate technique over a GaAs/AlGaAs heterostructure. The applied bias on the gates formed a square cavity with QPCs at right angles to one another. The self-consistent solution for the potential is a "stomach" shaped quantum dot (the shape can be inferred by the wave functions shown in the central panels of Fig. 3). The input and output QPCs of this dot support 2 propagating modes, assuming E_F ~14 meV (we use a variant of the cascading scattering matrix approach [13] to obtain the transmission coefficients which enter the Landauer-Büttiker formula to give the conductance and to calculate the wave functions). In our energy range of interest, this would be considered an open dot.

We have studied the influence of the closed dot spectrum and eigenstates on the open dot transport. To obtain this spectrum, we have taken the portion of the dot potential and placed it inside a 2D square well, so that the QPCs are blocked by infinite potential barriers and solve a 2D Schrödinger equation with Dirichlet boundary conditions. The point of closure is where the QPCs are at their narrowest. In the left panel of Fig. 3, we show the 55*th* through 75*th* eigenstates. Like states found in stadium billiard [14], many of these dot states have a disorganized, quasi-random look, which is to be expected, since this type of rounded potential is known to be classically chaotic. However, state 65 stands out. Not only is it symmetric, it appears to be scarred by a periodic orbit reminiscent of a "whispering gallery" trajectory noted in stadiums [15].

Since the closed dot states form an orthogonal basis set, the wave functions of an open dot can be expressed as a linear combination of these states by means of projection. In the top part of the central panel of Fig. 3, we plot the magnitude of the open dot wave function, $|\Psi(x,y)|$, coinciding to the energy of the 65*th* closed dot state. At this energy, there is a resonance in conductance. Not only does the open dot wave function closely resemble the close dot eigenstate but the decomposition (top right panel) indicates that, despite the fact that this dot is open, transport for the conduc-

tance resonance is mediated essentially by a single eigenstate. The bottom central panel corresponds to the open dot wavefunction coinciding to the energy of the 74*th* level. Unlike the previous example, the decomposition (lower right panel) shows that several eigenstates contribute to the open dot wave function. This is a situation where the closed dot state has in fact been broadened by opening the dot. We find that typically the states that tend to survive in the open situation are those that are scarred. These results indicate that a model that assumes uniform level broadening can not provide an accurate general description for the physics of open dots.

It should be noted that changing the QPC configuration (for example, having the QPCs aligned with each other) will change the set of states that are maintained in the open structure.

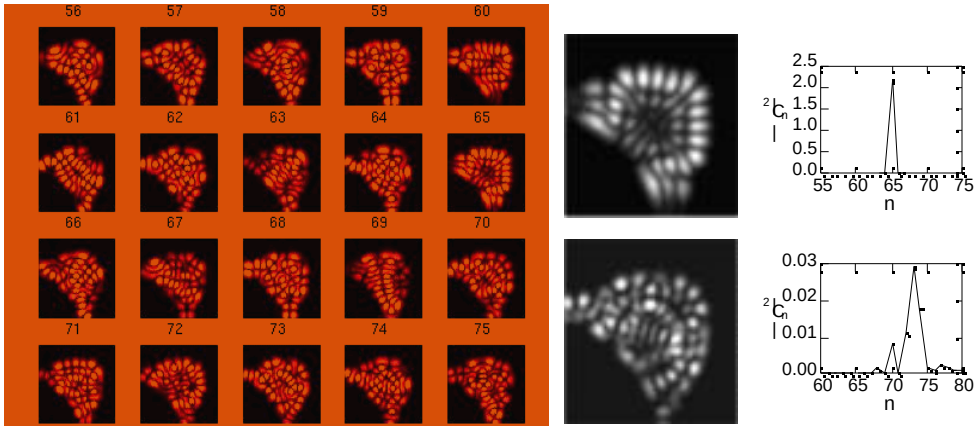

Figure 3: On the left are the 56*th* through 75*th* eigenstates (note that state 65 is scarred). In the center are two wavefunctions for an open quantum dot with two modes in the QPCs. The decompositions of these wavefunctions in terms of the closed dot eigenstates shown on the right indicates that scarred eigenstate survives even in the open system.

CONCLUSIONS

Simulation results for *n*-channel MOSFETs with 0.1 μm gate-length and 0.05 μm gate-width were presented that clearly show the fluctuations of the device transfer characteristics because of the different number and different distribution of the impurity atoms under the gate. Significant correlation between the threshold voltage and the number of dopants that fall within the first 30-40 nm from the SiO_2 interface was also observed. This suggests that an analysis that only takes into account the total number of atoms under the gate to describe fluctuations in the threshold will give misleading results.

Regarding open quantum dots, we have found that level broadening occurs in a very selective manner. This result has important implications on the applicability of random matrix theory in the study of quantum dots, as it relies on the assumption that the level structure is not preserved.

REFERENCES

[1] M.A. Read and W.P. Kirk, "Nanostructure Physics and Fabrication," Academic, Boston, 1989.

[2] A. Lorke, J.P. Kotthaus and K. Ploog, Phys. Rev. Lett. 64, 2559, 1990.

[3] D. Vasileska, W.J. Gross and D.K. Ferry, Proceedings of the 1998 Sixth International Workshop on Computational Electronics, 259, 1998.

[4] W.J. Gross, D. Vasileska and D.K. Ferry, submitted for publication in Electron Dev. Lett.

[5] D. Vasileska, M.N. Wybourne, S.M. Goodnick, A.D. Gunther, Semicond. Sci. Technol. 13, A37, 1998.

[6] D.K. Ferry, R. Akis, S. Udipi, D. Vasileska, D.P. Pivin, Jr., K.M. Connoly, J.P. Bird, K. Ishibashi, Y. Aoyagi, T. Sugano and Y. Ochiai, Jpn. J. Appl. Phys. 36, 1841, 1997.

[7] H. L. Stone, SIAM J. Numer. Anal. 5, 530, 1968.

[8] H. A. Van der Vorst, SIAM J. Sci. Stat. Comput. 13, 631, 1992.

[9] D. Vasileska, W.J. Gross, V. Kafedziski and D.K. Ferry, VLSI Design 8, 1-4, 301, 1998.

[10] M.Persson, J. Pettersson, B. von Sydow, P.E. Lindelof, A. Kristensen and K.F. Berggren, Phys. Rev. B, 52, 8921, 1995.

[11] K.F. Berggren, Z.-L. Li, T. Lundberg, Phys. Rev. B, 54, 11672, 1996.

[12] R.A. Jalabert, H.U. Baranger, and A.D. Stone, Phys. Rev. Lett. 65, 2442, 1990.

[13] T. Usuki, M. Saito, M. Takatsu, R.A. Kiehl, and N. Yokoyama, Phys. Rev. B, 52, 8244, 1995.

[14] S.W. McDonald, and A.N. Kaufman, Phys. Rev. A 37, 3067, 1988.

[15] E. J. Heller, P.W. O' Connor, and J. Gehlen, Phys. Scr. 40, 354, 1989.